



Fan Noise Source Diagnostic Test— Vane Unsteady Pressure Results

Edmane Envia
Glenn Research Center, Cleveland, Ohio

The NASA STI Program Office . . . in Profile

Since its founding, NASA has been dedicated to the advancement of aeronautics and space science. The NASA Scientific and Technical Information (STI) Program Office plays a key part in helping NASA maintain this important role.

The NASA STI Program Office is operated by Langley Research Center, the Lead Center for NASA's scientific and technical information. The NASA STI Program Office provides access to the NASA STI Database, the largest collection of aeronautical and space science STI in the world. The Program Office is also NASA's institutional mechanism for disseminating the results of its research and development activities. These results are published by NASA in the NASA STI Report Series, which includes the following report types:

- **TECHNICAL PUBLICATION.** Reports of completed research or a major significant phase of research that present the results of NASA programs and include extensive data or theoretical analysis. Includes compilations of significant scientific and technical data and information deemed to be of continuing reference value. NASA's counterpart of peer-reviewed formal professional papers but has less stringent limitations on manuscript length and extent of graphic presentations.
- **TECHNICAL MEMORANDUM.** Scientific and technical findings that are preliminary or of specialized interest, e.g., quick release reports, working papers, and bibliographies that contain minimal annotation. Does not contain extensive analysis.
- **CONTRACTOR REPORT.** Scientific and technical findings by NASA-sponsored contractors and grantees.

- **CONFERENCE PUBLICATION.** Collected papers from scientific and technical conferences, symposia, seminars, or other meetings sponsored or cosponsored by NASA.
- **SPECIAL PUBLICATION.** Scientific, technical, or historical information from NASA programs, projects, and missions, often concerned with subjects having substantial public interest.
- **TECHNICAL TRANSLATION.** English-language translations of foreign scientific and technical material pertinent to NASA's mission.

Specialized services that complement the STI Program Office's diverse offerings include creating custom thesauri, building customized data bases, organizing and publishing research results . . . even providing videos.

For more information about the NASA STI Program Office, see the following:

- Access the NASA STI Program Home Page at <http://www.sti.nasa.gov>
- E-mail your question via the Internet to help@sti.nasa.gov
- Fax your question to the NASA Access Help Desk at 301-621-0134
- Telephone the NASA Access Help Desk at 301-621-0390
- Write to:
NASA Access Help Desk
NASA Center for Aerospace Information
7121 Standard Drive
Hanover, MD 21076



Fan Noise Source Diagnostic Test— Vane Unsteady Pressure Results

Edmane Envia
Glenn Research Center, Cleveland, Ohio

Prepared for the
Eighth Aeroacoustics Conference
cosponsored by the American Institute of Aeronautics and Astronautics
and the Confederation of European Aerospace Societies
Breckenridge, Colorado, June 17–19, 2002

National Aeronautics and
Space Administration

Glenn Research Center

Acknowledgments

The experimental data used in this work were obtained through cooperation and support of many individuals from NASA Glenn Research Center, General Electric Aircraft Engines, and the Boeing Commercial Airplanes Group. The author is grateful for their efforts and dedication.

This report is a formal draft or working paper, intended to solicit comments and ideas from a technical peer group.

Available from

NASA Center for Aerospace Information
7121 Standard Drive
Hanover, MD 21076

National Technical Information Service
5285 Port Royal Road
Springfield, VA 22100

Available electronically at <http://gltrs.grc.nasa.gov>

Fan Noise Source Diagnostic Test - Vane Unsteady Pressure Results

Edmane Envia*
National Aeronautics and Space Administration
Glenn Research Center
Cleveland, Ohio 44135

Abstract

To investigate the nature of fan outlet guide vane pressure fluctuations and their link to rotor-stator interaction noise, time histories of vane fluctuating pressures were digitally acquired as part of the Fan Noise Source Diagnostic Test. Vane unsteady pressures were measured at seven fan tip speeds for both a radial and a swept vane configuration. Using time-domain averaging and spectral analysis, the blade passing frequency (BPF) harmonic and broadband contents of the vane pressures were individually analyzed. Significant Sound Pressure Level (SPL) reductions were observed for the swept vane relative to the radial vane for the BPF harmonics of vane pressure, but vane broadband reductions due to sweep turned out to be much smaller especially on an average basis. Cross-correlation analysis was used to establish the level of spatial coherence of broadband pressures between different locations on the vane and integral length scales of pressure fluctuations were estimated from these correlations. Two main results of this work are: (1) the average broadband level on the vane (in dB) increases linearly with the fan tip speed for both the radial and swept vanes, (2) the broadband pressure distribution on the vane is nearly homogeneous and its integral length scale is a monotonically decreasing function of fan tip speed.

Introduction

It has long been postulated that rotor-stator interaction noise is primarily generated by the pressure fluctuations that are induced on the stator vanes as a result of the impingement of the passing rotor wakes. These local pressure fluctuations, once produced, propagate outward and coalesce with the pressure waves originating elsewhere on the stator, to form a spinning pressure pattern known as a duct mode. If the conditions are favorable (as dictated by the duct geometry, mean flow characteristics and frequency of the fluctuations), these spinning pressure patterns are self-sustaining and result in the so-called propagating modes, which eventually radiate to the farfield from engine inlet and exhaust. Most of the time, however, due to imperfect phase and amplitude matching between their constituent elements, the modes are evanescent and decay in the fan duct and never make it to the farfield. The aggregate contributions from all these duct modes constitute the pressure field that is called the rotor-stator interaction noise.

This description of the underlying process is satisfactory (and useful) when dealing with coherent (i.e., periodic) vane fluctuations that result in discrete frequency interaction tones. In fact, noise reduction strategies that are predicated on this idea have shown to be effective (see, for example, [1]). However, when dealing with incoherent (i.e., broadband) vane pressure fluctuations, the picture is unwieldy since the notion of proper phase and amplitude matching is ill defined and one is hard-pressed to reconcile the random phase and amplitude characteristics of vane pressure fluctuations with specific well-defined mode patterns since this implies some measure of underlying order and coherence.

In an attempt to elucidate the connection between the vane pressure fluctuations and the rotor-stator interaction noise, surface distributions of vane fluctuating pressures were measured as part of the Fan Noise Source Diagnostic Test (SDT). The SDT was a comprehensive aero-acoustic test of a model 22-inch fan stage representing the bypass section of a modern high bypass ratio turbofan engine. In addition to the vane unsteady

* Aerospace Engineer, Senior Member, AIAA

pressures, blade row and stage aerodynamic performance data, fan inlet, tip flow and wake turbulence, fan duct wall fluctuating pressures, fan duct modes, and farfield noise spectra were also acquired as part of the SDT [2–8]. The tests were conducted in the NASA Glenn Research Center’s 9-foot by 15-foot acoustic wind tunnel. The model fan has 22 blades and a design tip speed of 1215 ft/sec. Three outlet guide vane (OGV) configurations were utilized in the SDT. A baseline OGV which has 54 radial vanes to “cut-off” the blade-passing-frequency (BPF) rotor-stator interaction tone, a low-count OGV representing a “cut-on” concept which has 26 radial vanes, and a swept OGV which has 26 swept vanes with 30 degrees of sweep. The smaller vane count for the 26-vane radial stator was selected to reduce broadband noise as compared with the baseline OGV [9]. The swept OGV was designed to minimize the blade passing frequency tone penalty associated with a cut-on vane design. All three stator had the same solidity.

Vane Unsteady Pressure Measurements

Vane pressure time histories were obtained using only the 26-vane radial and swept OGVs shown in Figure 1. Owing to its relatively small chord and thickness, the baseline stator was unsuitable for instrumentation. For each of the two tested stator configurations, there were two instrumented vanes: one (designated vane 1) containing 31 pressure transducers and its neighbor (designated vane 2) containing only 11 pressure transducers. The transducers were arranged in three chordwise lines (at the 20%, 60% and 87% span locations) and one spanwise line (at 20% chord location). The locations and layout of the sensors are shown in Figure 2. The transducer layout was chosen to maximize the vane surface area coverage given the physical limitations that existed in the total number of the transducers that could be accommodated inside the vane.

The transducers were encased within the vanes, which were split along the 40%–60% thickness line to accommodate the transducers as shown in Figure 3. The transducers were vented on both sides so they measured the pressure difference fluctuations across the blade thickness. However, by taping one side of the vane, pressure-side or suction-side fluctuations could also be measured.

Unsteady pressure data for seven fan tip speeds (see Table 1) were recorded for later analysis. In this paper, mainly, the results for three fan speeds, 61.7%, 87.5% and 100%, will be presented. These speeds correspond to the approach, cutback and takeoff conditions for the model fan stage. However, where appropriate, significant results for all tested tip speeds will be shown.

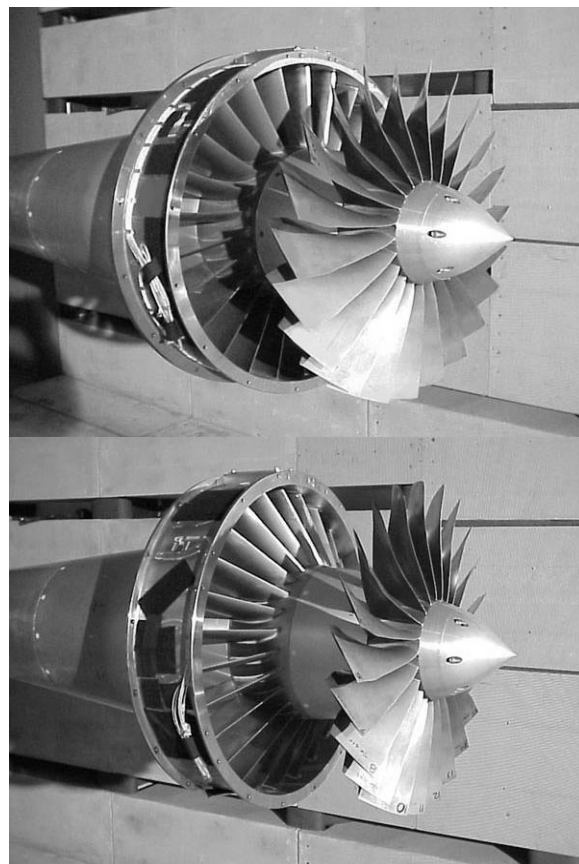


Figure 1. Photographs of partially assembled 22-inch Source Diagnostic Test fan stage. The fan outlet guide vane stators for which surface unsteady pressure data were obtained are shown. (Top: 26-vane radial stator. Bottom: 26-vane swept stator).

For each test condition, 9.6 seconds of pressure time histories were digitally recorded at a sampling rate of 128 kHz for all transducers simultaneously. Since, the fan rpm tended to drift slightly (typically less than $\pm 0.3\%$) during each run, the recorded data had to be resampled (via interpolation) assuming a fixed nominal (average) rpm. By a judicious choice of resampling rate, the interpolation error was minimized.

The resulting re-sampled data was then ensemble-averaged (in the time-domain) to separate the periodic and non-periodic parts of the signal. By choosing the ensemble size to correspond to one revolution of fan shaft, the periodic part could be made to include all coherence that is shaft-order locked (i.e., it is synchronous to the once-per-revolution dynamics). This includes not only the components that are related to the blade passing frequency (BPF) harmonics, but also any periodicity associated with the blade-to-blade variations. Subtracting the periodic part from the original time trace yields a time series that is an aggregate of all components that are not periodic in any shaft order. The shaft-order locked time

series was further averaged over the period for one blade passage to isolate the BPF harmonic content. The resulting three constituent time series, i.e., the broadband, shaft-orders and BPF harmonics, could then be individually analyzed on a spectral basis. The time averaging was done using a large number of contiguous ensembles (over 1000 for all cases) to ensure good averages. A representative example of the resulting “decomposed” spectra is shown in Figure 4. The overall and the constituent broadband and shaft order Sound Pressure Level (SPL) spectra are plotted with the BPF harmonic content superimposed on the shaft orders for clarity. All of the results presented in this paper were obtained using this procedure.

The presentation of the test results is as follows. BPF harmonic data are presented first and are followed by the broadband data. In each case, sample results are shown and discussed with additional relevant results included in two appendices at the end of the paper. Since,

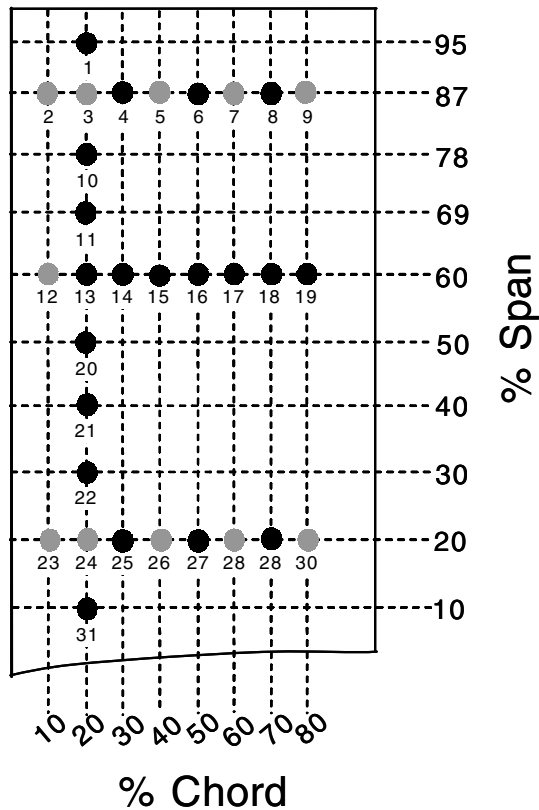


Figure 2. Layout of vane pressure transducer locations for the radial stator. Two adjacent vanes were instrumented. There were 31 pressure transducers on vane 1 and 11 pressure transducers on vane 2. Dark circles indicate pressure transducer locations on vane 1 only. Light circles denote pressure transducers locations on both vanes. The swept vane had an identical layout on percent basis.

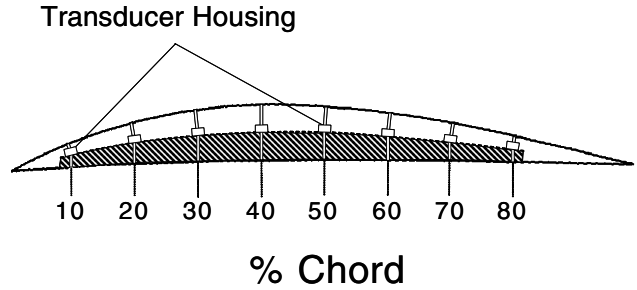


Figure 3. Schematic of vane-embedded pressure transducer locations. Pressure transducers were located along the 40%–60% thickness split line. (Not to scale).

% Design Tip Speed	Nominal RPM _{Corrected}	Condition
50.0		
61.7	7808	Approach
75.0		
87.5	11074	Cutback
90.0		
100.0	12656	Takeoff
100.7		

Table 1. Fan conditions used in the vane unsteady pressure measurements. The highlighted speeds are the ones for which most of the results in this paper are presented.

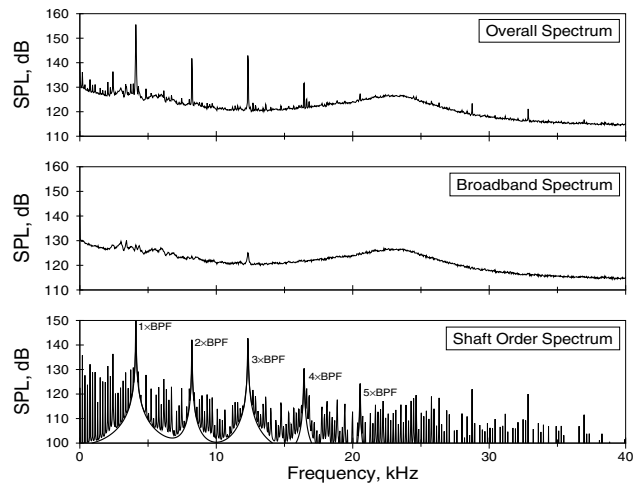


Figure 4. Spectral decomposition via time-domain averaging. Representative results for the radial stator at 87.5% tip speed are shown. The spectrum of the original time series is on the top and that for its broadband content in the middle. On the bottom, are the shaft order and BPF harmonic spectra plotted together. Note the preponderance of shaft order harmonic content present in the time series.

the vane 2 data turned out to be similar in character to the vane 1 data, only results for the 31 transducers on vane 1 will be included here. In all but a few cases, the results are plotted on the percent span and percent chord basis to facilitate comparison of the radial and swept vane results. Also, unless otherwise stated, the results shown are for the unsteady pressure difference across the vane, that is for $\Delta p = (p_{suction} - p_{pressure})$.

BPF Harmonic Results

The 1xBPF harmonic magnitude and phase of the vane unsteady pressure at the approach condition are shown in Figures 5 and 6 for both the radial and swept vanes. The presentation of the results follows the layout of the transducers shown in Figure 2. To save space, the spanwise plot (i.e., the graph on the left) is turned on its side so that the ordinate and abscissa are interchanged. The BPF harmonic SPL is in dB and its phase (un-rolled if necessary) is in degrees. The solid lines denote the radial vane results and the dashed lines the swept vane results. In the forward portion of the vane ($< 30\%$ chord), there are noticeable reductions in the SPL (by as much as 10 dB) due to vane sweep, but as one moves further aft along the chord, the sweep benefits diminish and there are even increases for the swept vane in a few places. These increases turn out to be incidental since an examination of corresponding results for the 2xBPF content at cutback and 3xBPF content at takeoff, shown in Figures A1 and A3 in Appendix A, indicate that vane sweep is almost always beneficial in reducing the level of vane pressure BPF harmonics.

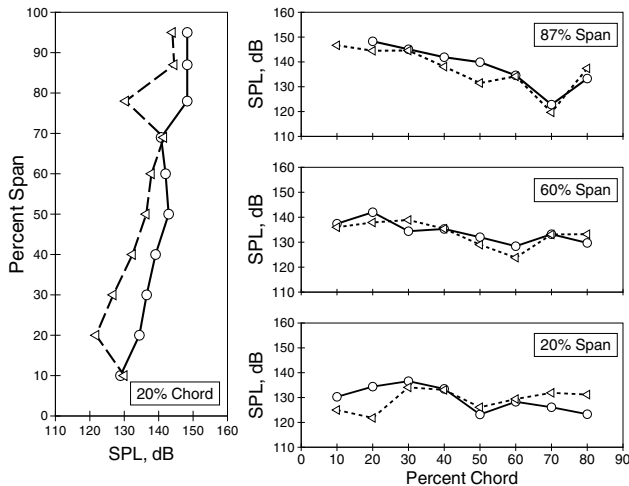


Figure 5. Influence of sweep on 1xBPF content of vane unsteady pressure. Solid lines denote SPL for the radial vane and dashed lines for the swept vane. Levels for the approach condition are shown.

The more puzzling result is the behavior of the phase of the BPF harmonics shown in Figure 6. Earlier studies (see, for example, [10]) had indicated that vane sweep is effective because it increases the obliqueness of the rotor wake as seen by the stator and thus increases the spanwise variation of the phase of the incident upwash and, as a consequence, the phase of the resultant unsteady pressure on the vane. In contrast, a comparison of the radial and swept vane BPF harmonic phases plotted in Figures 6, A2 and A4 in fact show comparable behavior for both vane configurations. One possible explanation for this unexpected behavior is that spanwise variation of the upwash once imprinted on the vane leading edge does not persist for any significant distance along the chord owing to the three dimensional nature of the unsteady pressure response. It is also possible that the spanwise arrangement of the transducers is too sparse to capture the details even if there is a significant variation in the phase along the span.

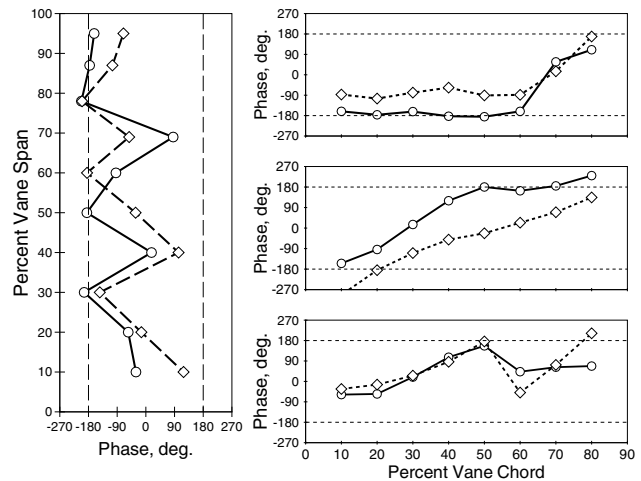


Figure 6. Comparison of 1xBPF spanwise and chordwise phase distributions for the radial (solid lines) and swept (dashed lines) vanes. Results for the approach condition are shown.

Next the dependence of the BPF harmonic content on the fan tip speed is examined. The SPL for the first five BPF harmonics obtained at three representative transducers (3, 13 and 24) are shown in Figure 7 for the radial vane and in Figure 8 for the swept vane. The solid bars denote the levels for approach, open bars for cutback and shaded bars for takeoff. Other than the absolute level differences between the radial and swept vane levels, the behavior of the harmonic content is similar for both showing that, for the most part, the SPL decreases monotonically with increasing harmonic order for all three spanwise locations and for all three speeds. The fall off rate for the harmonic amplitudes depends on the fan tip speed and is large at approach and much smaller at takeoff. This is likely a result of the change in the

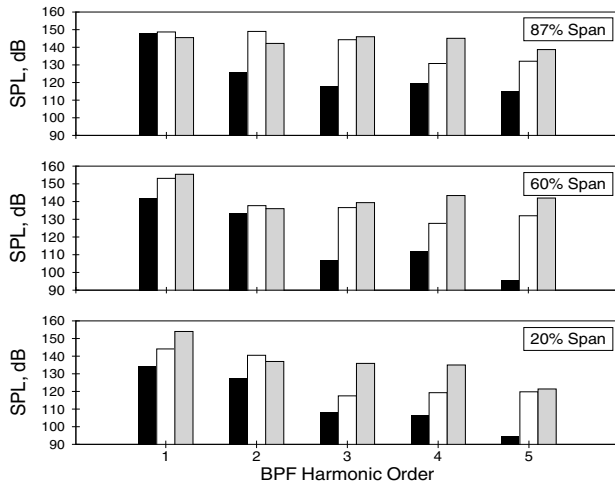


Figure 7. Influence of fan tip speed on BPF harmonics of the vane unsteady pressure for transducers 3, 13 and 24. Solid bars denote levels at approach, open bars the levels at cutback and shaded bars the levels at takeoff. The results shown are for the radial stator.

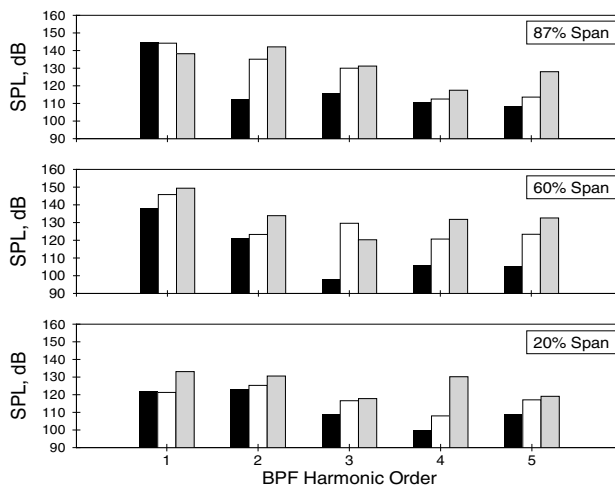


Figure 8. Same as Figure 7 but with the results for the swept stator shown.

magnitude of the circumferential phase velocity of the rotor disturbances as they pass the stator vanes. As the tip speed of the fan is increased, the circumferential phase speed of the disturbances increases producing “sharper” waveforms for the unsteady vane pressures. The sharper waveforms have more evenly distributed BPF harmonic content as compared with the smoother waveforms at the approach condition.

The differences between the BPF harmonic magnitude and phase for the taped and un-taped vane configurations are shown in Figures 9 through 12. Recall that by taping one side of the vane, pressure histories on the opposite side could be obtained. The taped side for

vane 1 was the suction side, so the corresponding results are for the pressure-side fluctuations denoted by $p_{pressure}$. The results for the untaped vane are denoted by Δp . In Figures 9 and 10, the 1xBPF magnitude and phase for the radial vane at the approach condition are shown. The corresponding results for the swept vane are shown in Figures 11 and 12. In these plots the solid lines denote the Δp results and dashed lines the $p_{pressure}$ results.

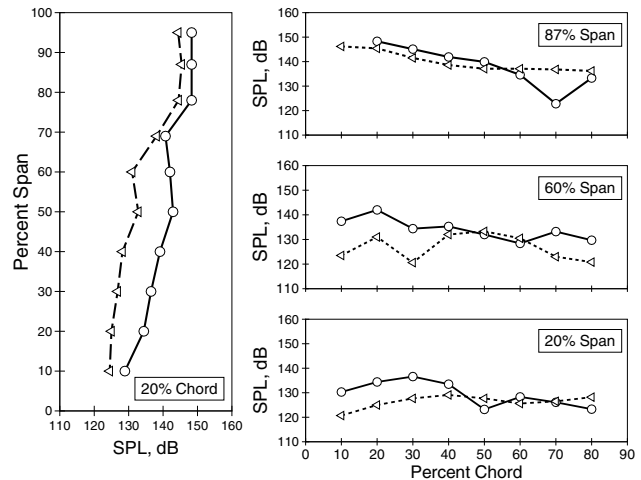


Figure 9. Comparison of 1xBPF SPL for the Δp (solid lines) and $p_{pressure}$ (dashed lines) configurations for the radial vane. Levels for the approach condition are shown.

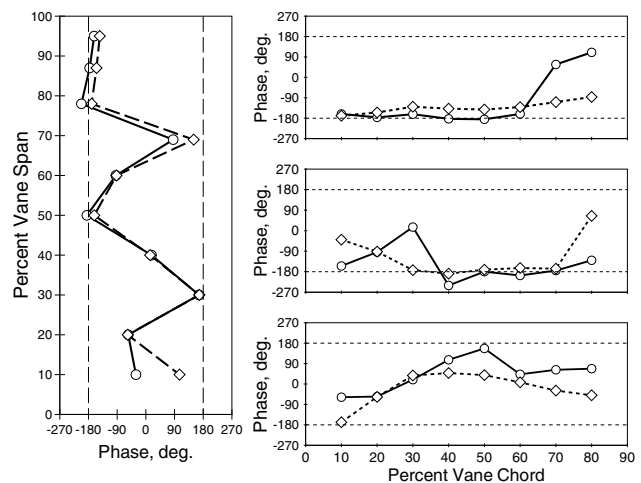


Figure 10. Comparison of 1xBPF phases for the Δp (solid lines) and $p_{pressure}$ (dashed lines) configurations for the radial vane. Levels for the approach condition are shown.

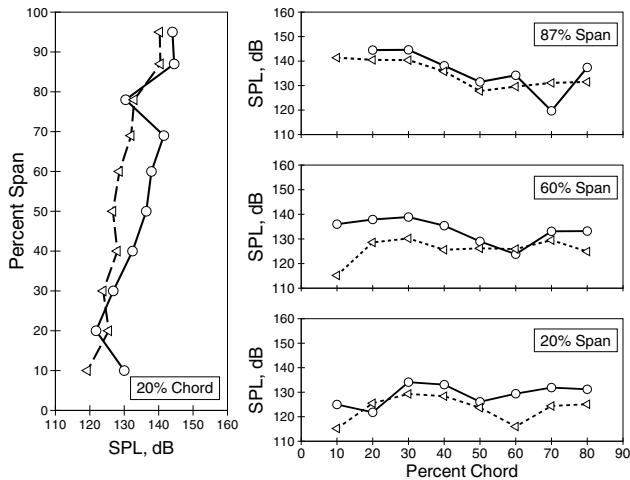


Figure 11. Same as Figure 9 but with the results for the swept vane shown.

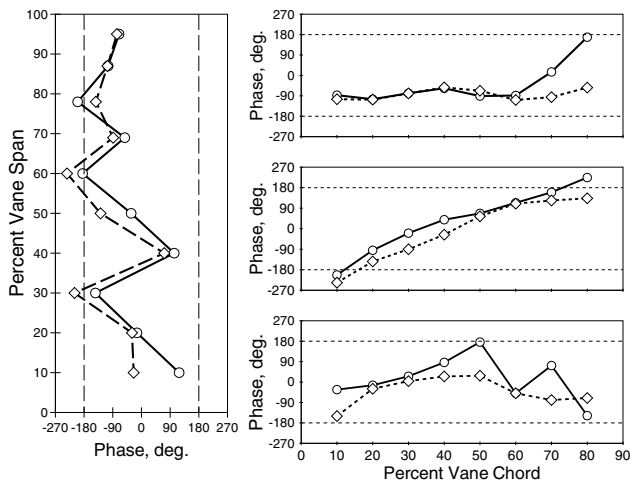


Figure 12. Same as Figure 10 but with the results for the swept vane shown.

In general, where the magnitudes and phases for the Δp and $p_{pressure}$ results are very close, the suction side levels must be small in comparison with the pressure side levels. However, where there are large differences between the two results, the picture is not as clear, since phase plays a much more important role. For example, if the pressure and suction side levels were nearly equal in amplitude but were out of phase, the resulting pressure difference would have twice the magnitude of each side. But if the two sides were in phase, then the Δp levels would be very small. Therefore, no general conclusions can be drawn from these results. The corresponding results for 2xBPF and 3xBPF content at cutback and approach are summarized in Figures A5 through A12.

Broadband Results

The presentation of broadband results is in two parts. In the first part, the presentation closely follows that for the BPF harmonic results except that the variations of broadband SPL are now plotted for all transducers on vane 1 as a function of various parameters. Here, the broadband SPL is defined to be the r.m.s value of pressure spectrum from 0 to 64 kHz with the latter being the Nyquist limit of the sampling rate. It should be noted that when the frequency range was truncated to 2 to 64 kHz to avoid all potential low-frequency contamination, the resulting r.m.s value changed by less than 0.5 dB. So, in what follows (and where applicable) the r.m.s value is based on the 0 to 64 kHz range. It should be noted that all spectra were computed using 600 overlapped 4096-point FFT ensembles in the frequency domain resulting in a bandwidth of 31.25 Hz for all cases presented.

In the second part of the presentation of broadband results, the nature of broadband pressure correlations on the vane and spatial coherence and integral length scales of broadband pressure are examined. As before, sample results are discussed in some detail with the additional relevant results included in Appendix B.

Figure 13 shows the influence of sweep on vane broadband levels at the approach condition. The corresponding results for the cutback and takeoff conditions are shown in Figures B1 and B2 in Appendix B. To begin with, note that for the most part there are broadband level reductions due to sweep but that these reductions are very modest typically 2 dB or less. For both vanes, however, there is an increase in the broadband level from hub to tip. For the approach condition, the

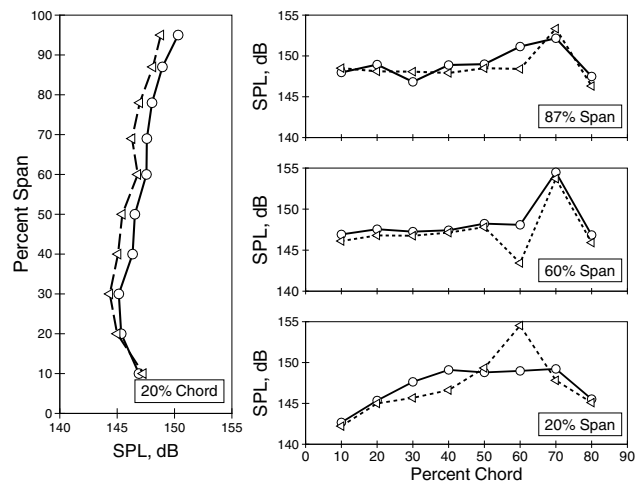


Figure 13. Influence of sweep on vane broadband level. Solid lines denote r.m.s broadband SPL for the radial vane and dashed lines for the swept vane. Levels for the approach condition are shown.

increase is as much as 5 dB, but for cutback and takeoff the increase is 2 dB or less. For the forward portion of the vane (say, less than 50% chord) the broadband levels stay essentially constant, but toward the trailing edge relatively large excursions in the broadband level are observed for all three speeds. The origin of these excursions is not clear. Overall, the data indicate that as the tip speed increases the variation of broadband SPL across the vane diminishes as does the difference between the radial and swept vane levels.

In Figures 14 and 15, the broadband Δp and $p_{pressure}$ levels are plotted for the radial and swept vanes, respectively. The pressure-side levels are generally lower by an average of 3 dB across the board. The likely reason is that the suction-side pressure loading is somewhat larger than the pressure-side loading. Corresponding result for the cutback and approach conditions can be found in Appendix B (Figures B3 through B6).

The influence of fan tip speed on the average broadband level for the radial and swept vanes is shown in Figure 16. In this figure the arithmetic average of the r.m.s levels of all vane transducers is plotted against the percent fan tip speed. Interestingly, the average broadband level (in dB) increases almost linearly with the fan tip speed. Evidently, the vane broadband loading is, on an average basis, a simple function of fan tip speed. Note also that the radial and swept vane levels are virtually the same in this average sense for any fan tip speed. This is a striking result, since the BPF harmonic content is reduced for the swept vane, but the average broadband is evidently not strongly affected by sweep!

Equally interesting is how this average level is related to the average farfield broadband level. As part of the vane unsteady pressure test, pressure time histories were simultaneously obtained at four microphone positions shown in Figure 17 (labeled as the reference wall and fixed microphones). These microphones were located approximately four fan diameters from the fan axis and a similar distance downstream of the fan exhaust nozzle. The average exhaust farfield broadband pressure levels, also plotted in Figure 16, show the same general trend as the vane average levels. Therefore, in an average sense, the vane and farfield broadband levels seem to be strongly linked.

The average broadband levels for the taped radial and swept vanes are compared with the corresponding farfield average levels in Figures B7 and B8. Consistent with the results already shown in Figures 13 and 14, the swept vane average broadband levels are very close to the radial vane levels, and the $p_{pressure}$ average broadband

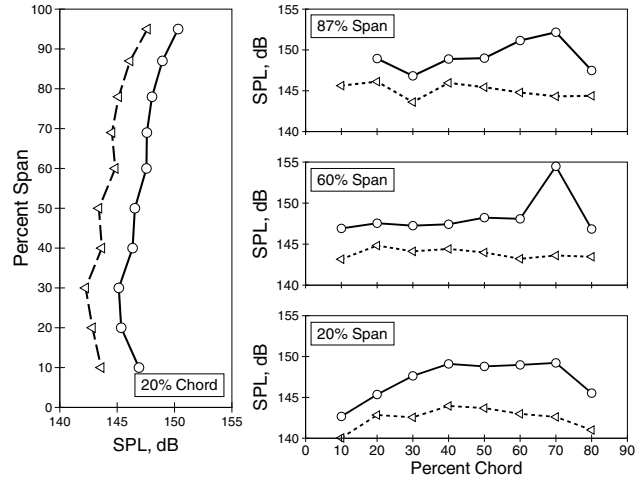


Figure 14. Comparison of the Δp (solid lines) and $p_{pressure}$ (dashed lines) r.m.s broadband levels for the radial vane. Levels for the approach condition are shown.

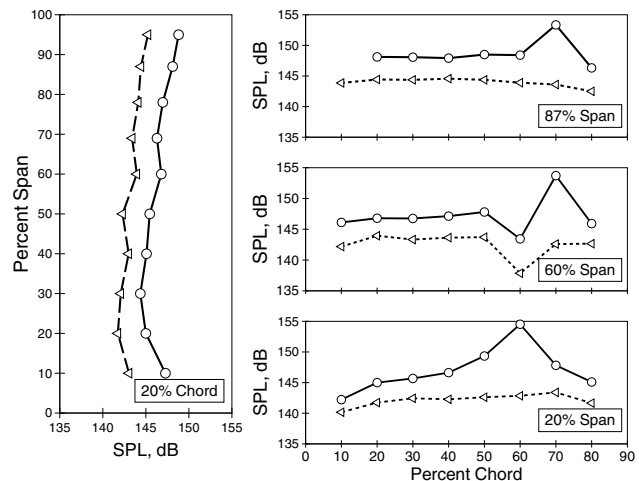


Figure 15. Same as Figure 14 but with the results for the swept vane shown.

SPL is consistently less than the corresponding Δp average broadband SPL.

Aside from examining the broadband pressure levels on the vane, the pressure time series were also used to establish the level of coherence between pressure fluctuations measured at different points on the vane. This was accomplished by computing the correlation coefficient $\rho_{i,j}(\tau)$ (see, for example, [11]) which defines the normalized cross-correlation between pressure fluctuations at a pair of points (i and j) at a given time delay τ . Naturally, the vane pressure fluctuations contain both convective (i.e., flow) and acoustic (i.e., sound) influences. Fortunately, since the time scales of the two

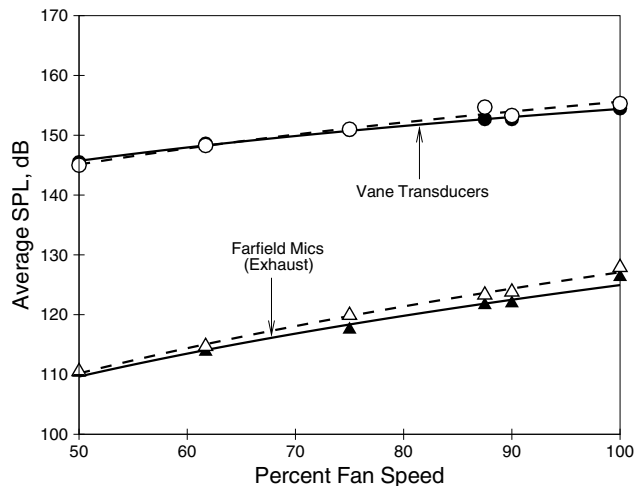


Figure 16. Dependence of vane average broadband SPL on fan tip speed for radial (solid line) and swept (dashed line) vanes. For comparison, the corresponding average broadband levels in the farfield (exhaust quadrant) are also plotted.

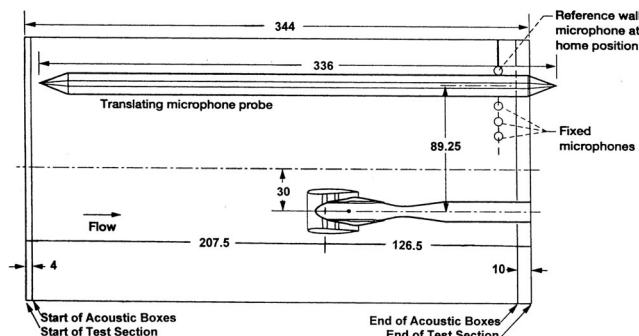


Figure 17. Location of the four farfield microphones for which pressure fluctuations were acquired simultaneously with the vane pressures. These are labeled the reference wall and fixed microphones.

processes are disparate, useful information can be extracted from such correlations. Computationally, it is most convenient to use the already computed individual broadband pressure spectra to construct the cross-spectrum in the frequency domain and then Fourier invert the result to obtain the cross-correlation in the time domain. The result is correlation over a whole range of time delays.

Typical results using this procedure are shown in Figure 18 where the correlation coefficient for a pair of transducer locations is plotted against a range of time delays (in msec) as their separation distance is increased. It should be emphasized that these results show the level of correlation between the broadband content of vane pressure only. Not surprisingly, the correlation level

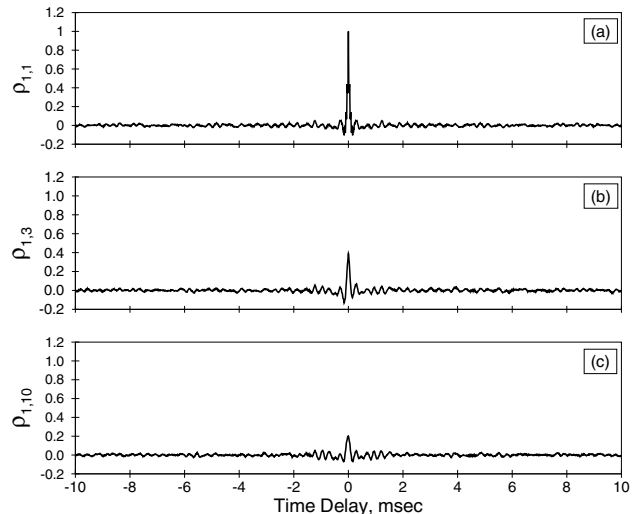


Figure 18. Correlations coefficient of the vane broadband pressure computed for three spanwise points at 20% chord: (a) is the auto-correlation coefficient of pressure at a reference point and (b) and (c) are the cross-correlations coefficients between the reference position with points, respectively 0.45 inch and 0.98 inch away. The results for the radial stator at the approach condition are shown.

diminishes as the spacing between the points is increased. Note also that highest levels of correlation occur at or near zero time delay, which suggests that the coherence is dominated by the acoustic rather than convective effects (large propagation speed resulting in small time delays).

The level of spatial coherence for broadband pressure at a given point on the vane surface can be estimated by considering the zero time delay correlation level as a function of separation distance along the span and chord lines passing through the point under consideration. The resulting plot typically looks like the example shown in Figure 19. It is clear that there is little difference between the spatial coherence in the spanwise and chordwise directions at this point indicating a homogeneous pressure field at that location.

The area under the curves in Figure 19 is the integral length scale of pressure. The variations of the chordwise and spanwise integral scales as a function of the span are shown in Figure 20 for both radial and swept vanes at the approach condition. These results indicate that the pressure field is essentially homogeneous showing only modest variation in the integral length scale across the vane. This is most likely due to the global nature of pressure field as opposed to the local nature of a turbulent eddy. Even a small turbulent eddy impinging on the vane will set up a pressure response everywhere on the stator. For the same reason, vane sweep does not seem to have a significant influence on the integral length scale either.

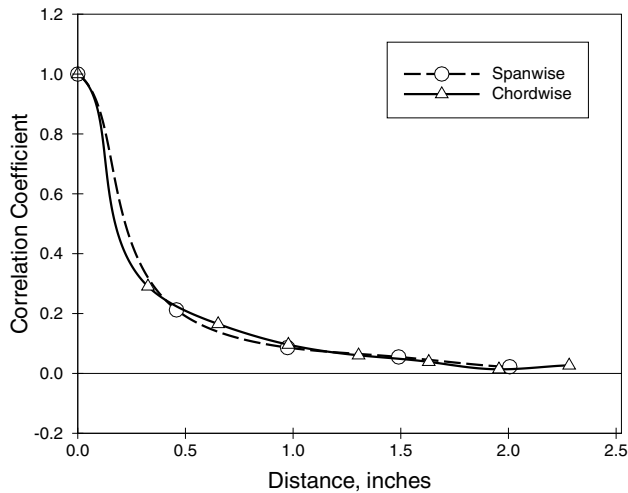


Figure 19. Variation of vane pressure zero-time-delay correlation with distance (typical result). Solid line denotes the variation along the span and dashed line variation along the chord for a given point on the vane. The results shown are for the radial vane at the approach condition.

Finally, the variation of the pressure integral scale as a function of fan tip speed is shown in Figure 21. The results indicate that the integral length scale of vane pressure decreases monotonically with increasing fan tip speed. This is probably because there is a corresponding decrease in the average size of the turbulence eddies impinging on the vane as the fan tip speed is increased. This conjecture cannot be verified until variation of the integral length scale(s) of turbulence interacting with the vane is measured as a function of tip speed.

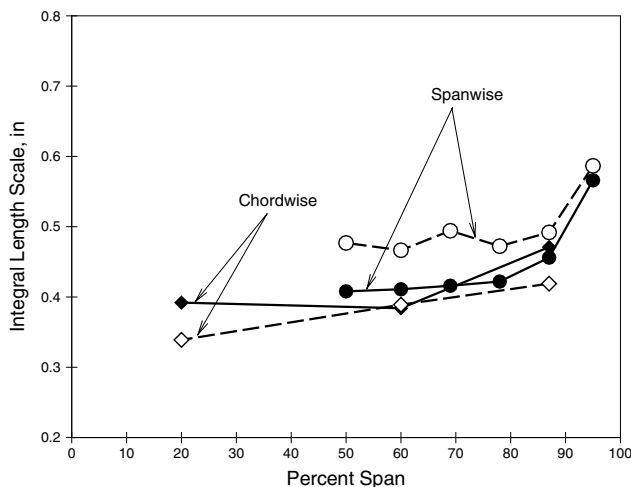


Figure 20. Spanwise variation of pressure integral length scales. Both spanwise (circles) and chordwise (diamonds) length scales are plotted. Radial vane results are denoted by solid symbols and swept vane results with open symbols.

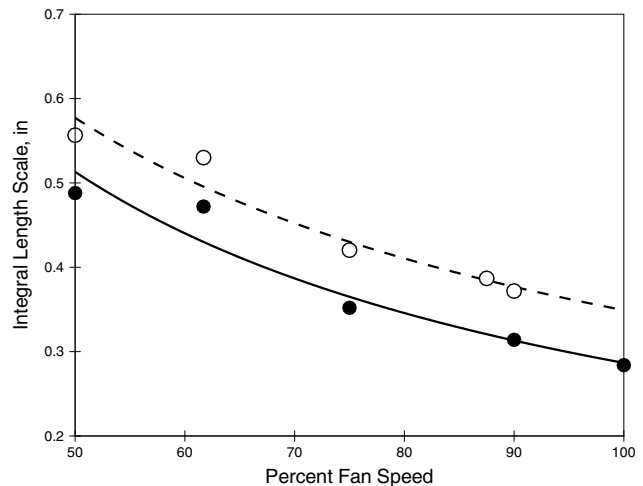


Figure 21. Dependence of integral length scale of pressure on fan tip speed. The results for radial vane (solid symbols) and swept vane (open symbols) are shown.

Summary

The nature of fan outlet guide vane pressure fluctuations was examined by acquiring digital samples of time histories of fluctuating pressures using instrumented vanes. Unsteady pressures were measured at seven fan tip speeds for both a radial and a swept vane configuration. Using time-domain averaging and spectral analysis, the blade passing frequency harmonic and broadband contents of the vane pressures were individually analyzed. Significant SPL reductions were observed for the swept vane relative to the radial vane for the BPF harmonics of vane pressure, but vane broadband reductions turned out to be much smaller especially on an average basis. Cross-correlation analysis was used to establish the level of spatial coherence of broadband pressures between different locations on the vane and the integral length scale of pressure fluctuations was estimated from these correlations. Two main results of this work are: (1) the average broadband level on the vane (in dB) increases linearly with the fan tip speed for both the radial and swept vanes, (2) the broadband pressure distribution on the vane is nearly homogeneous and its integral length scale is a monotonically decreasing function of fan tip speed.

Appendix A

Additional Tone Results

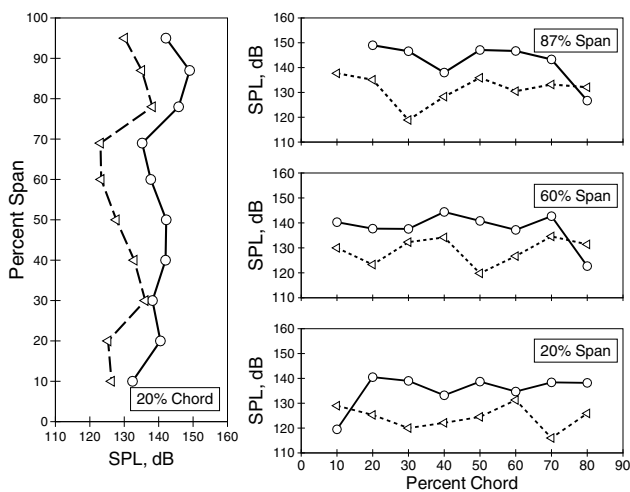


Figure A1. Influence of sweep on 2xBPF harmonic content of vane unsteady pressure. Solid lines denote SPL for the radial vane and dashed lines for the swept vane. Levels for the cutback (87.5% tip speed) condition are shown.

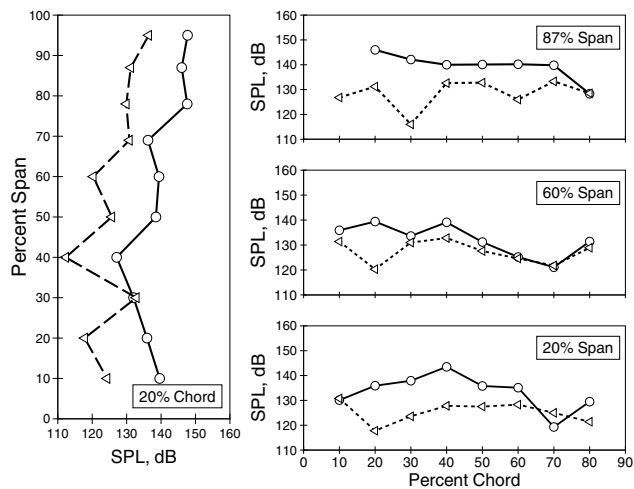


Figure A3. Same as Figure A1 but with 3xBPF harmonic levels at the takeoff (100.0% tip speed condition) shown.

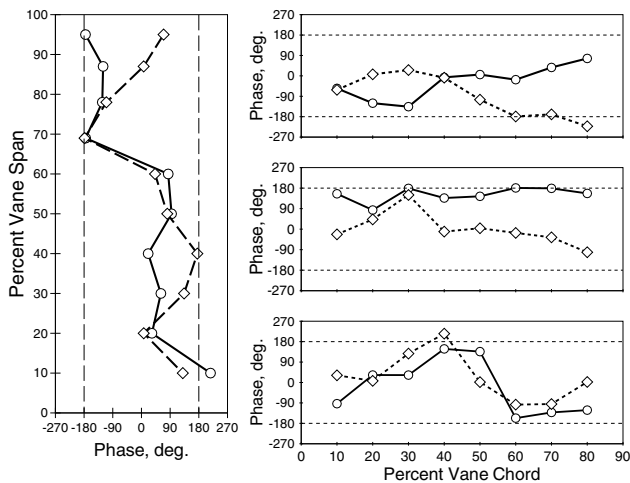


Figure A2. Comparison of 2xBPF spanwise and chordwise phase distributions for radial (solid lines) and swept (dashed lines) vanes. Results for the cutback condition are shown.

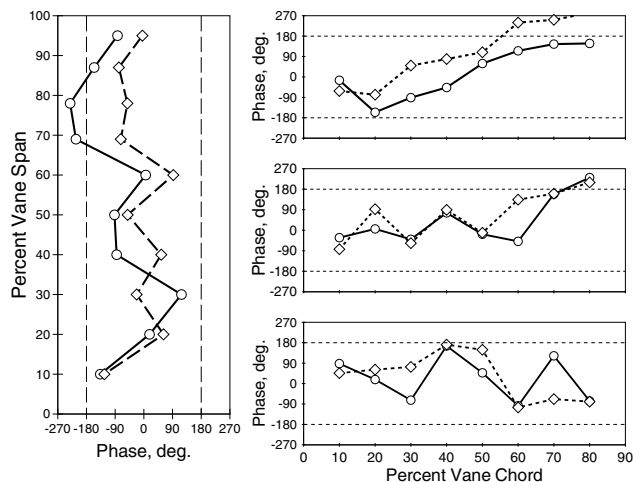


Figure A4. Same as Figure A2 but with 3xBPF phases at the takeoff condition shown.

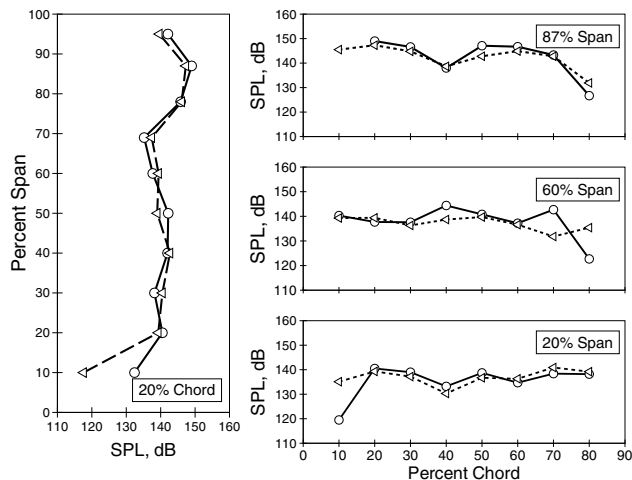


Figure A5. Comparison of 2xBPF SPL for the Δp (solid lines) and $p_{pressure}$ (dashed lines) configurations for the radial vane. Levels for the cutback condition are shown.

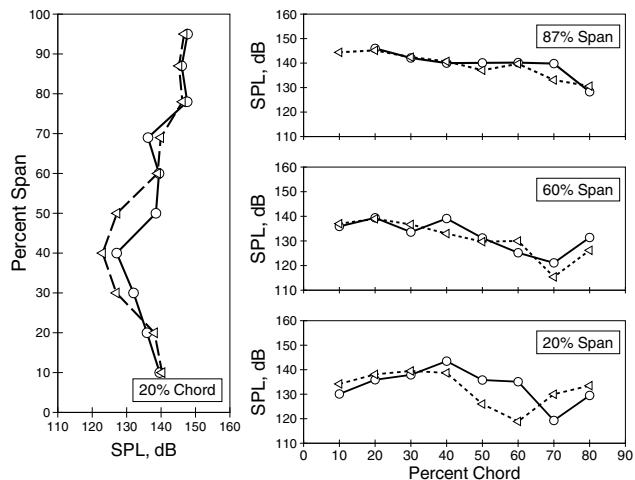


Figure A7. Same as Figure A5 but with 3xBPF levels for the takeoff condition shown.

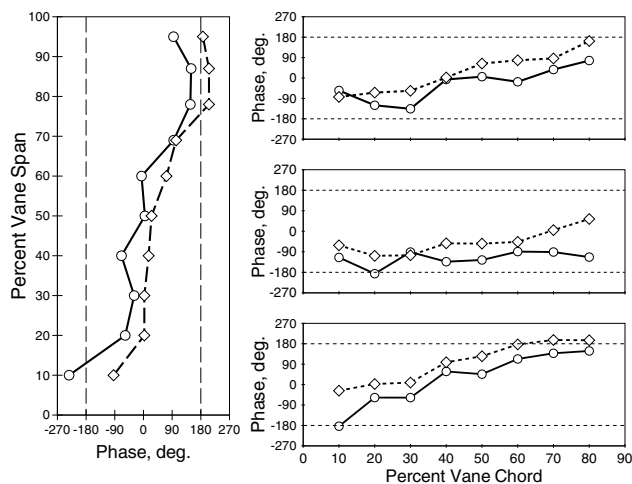


Figure A6. Comparison of 2xBPF phase for the Δp (dashed line) and $p_{pressure}$ (solid lines) configurations for the radial vane. Levels for the cutback condition are shown.

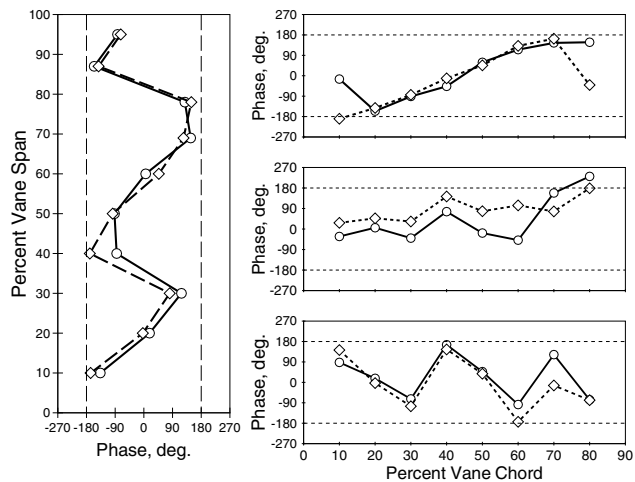


Figure A8. Same as Figure A6 but with 3xBPF phases for the takeoff condition shown.

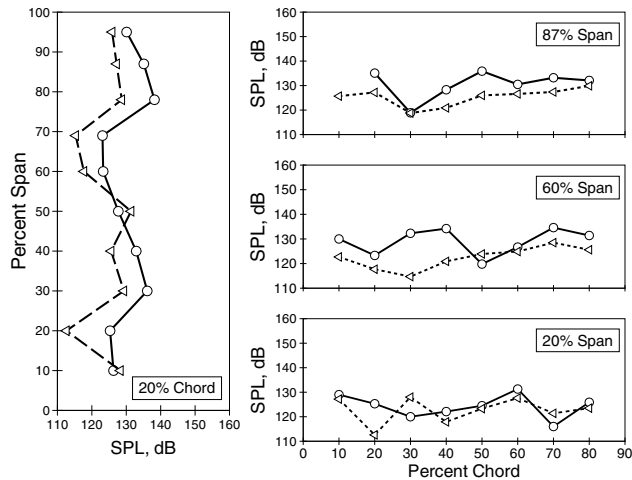


Figure A9. Comparison of 2xBPF SPL for the Δp (solid line) and $p_{pressure}$ (dashed line) configurations for the swept vane. Levels for the cutback condition are shown.

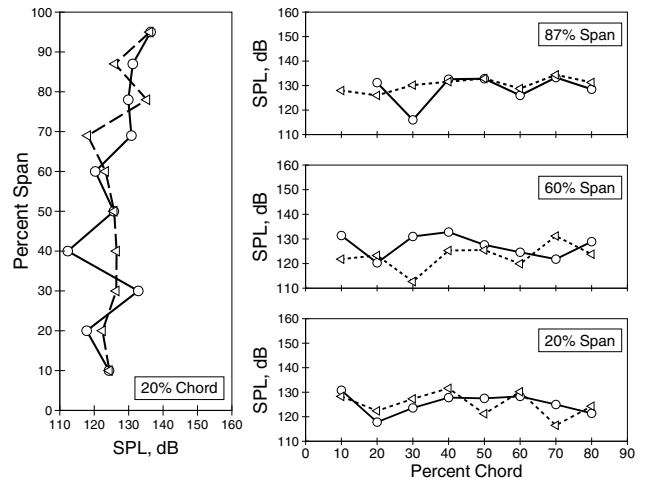


Figure A11. Same as Figure A9 but with 3xBPF levels for the takeoff condition shown.

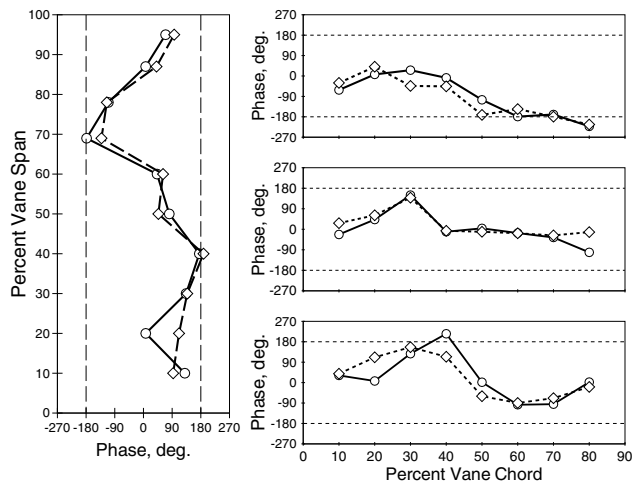


Figure A10. Comparison of 2xBPF phases for the Δp (solid line) and $p_{pressure}$ (dashed line) configurations for the swept vane. Levels for the cutback condition are shown.

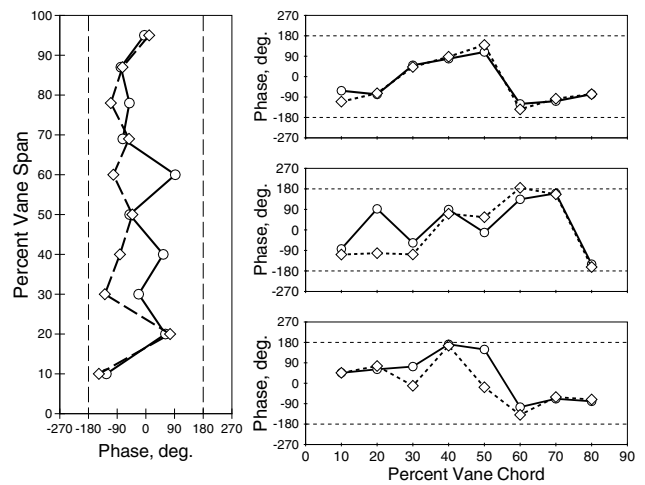


Figure A12. Same as Figure A10 but with 3xBPF levels for the takeoff condition shown.

Appendix B

Additional Broadband Results

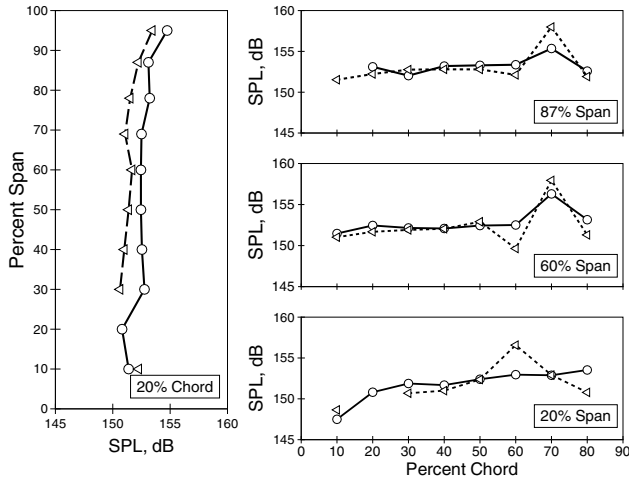


Figure B1. Influence of sweep on vane broadband level. Solid lines denote r.m.s broadband SPL for the radial vane and dashed lines for the swept vane. Levels for the cutback condition are shown.

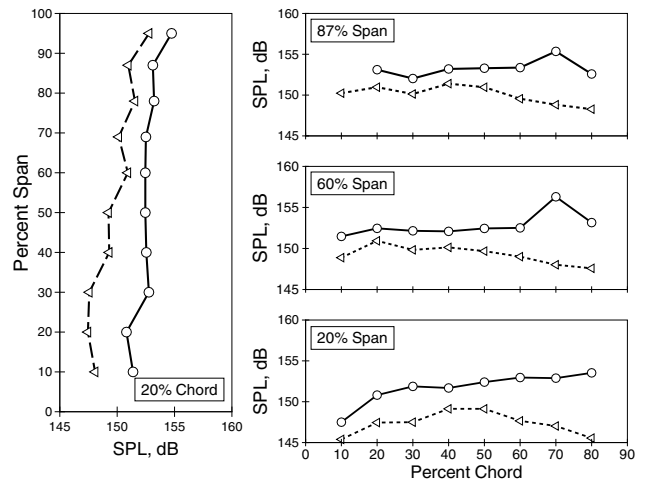


Figure B3. Comparison of the Δp (solid lines) $p_{pressure}$ (dashed lines) r.m.s broadband levels for the radial vane. Levels for the cutback condition are shown.

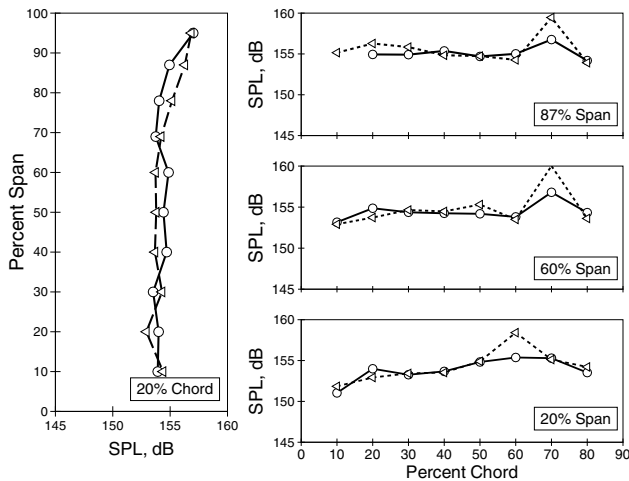


Figure B2. Same as Figure B1 but with r.m.s broadband levels at the takeoff condition shown.

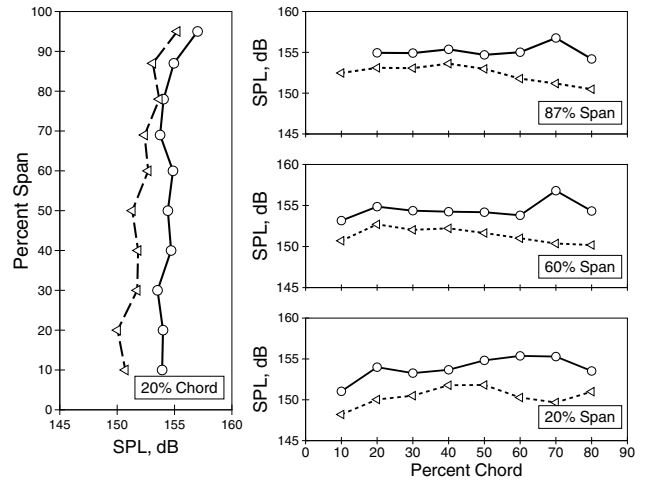


Figure B4. Same as Figure B3 but with r.m.s broadband levels at the takeoff condition shown.

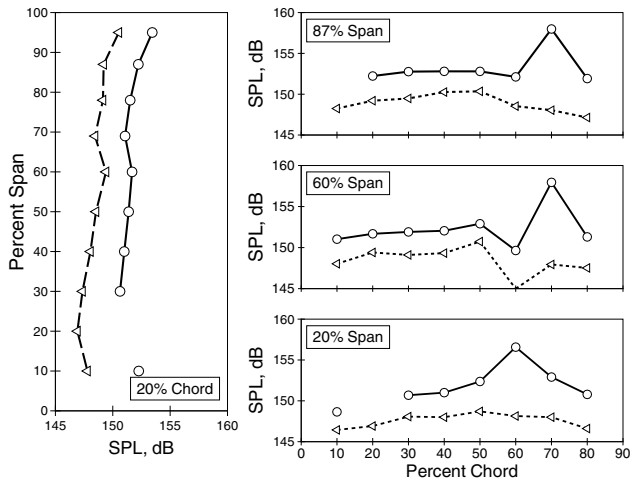


Figure B5. Comparison of the Δp (solid lines) and $p_{pressure}$ (dashed lines) r.m.s. broadband levels for the swept vane. Levels for the cutback condition are shown.

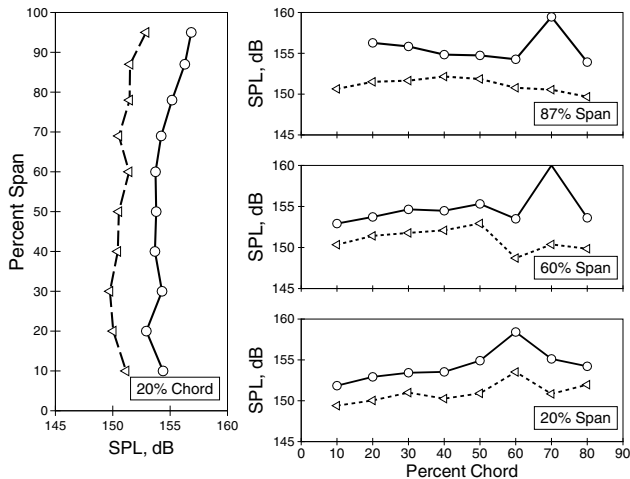


Figure B6. Same as Figure B5 but with broadband levels at the takeoff condition shown.

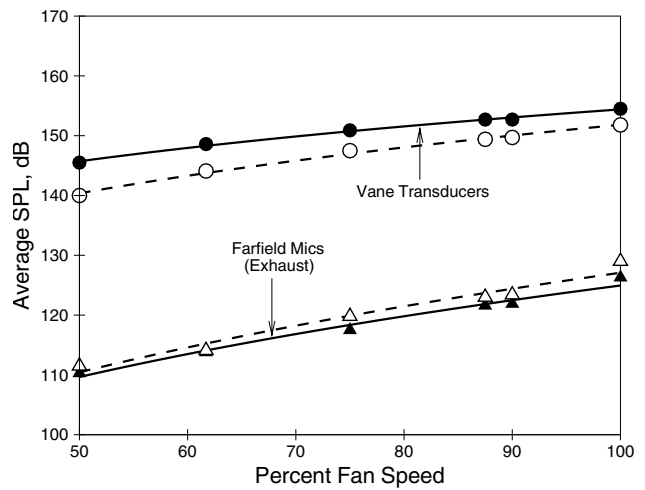


Figure B7. Dependence of vane average broadband SPL on fan tip speed for the Δp (solid lines) and $p_{pressure}$ (dashed lines) configurations shown for the radial vane. For comparison, the corresponding average broadband levels in the farfield (exhaust quadrant) are also plotted.

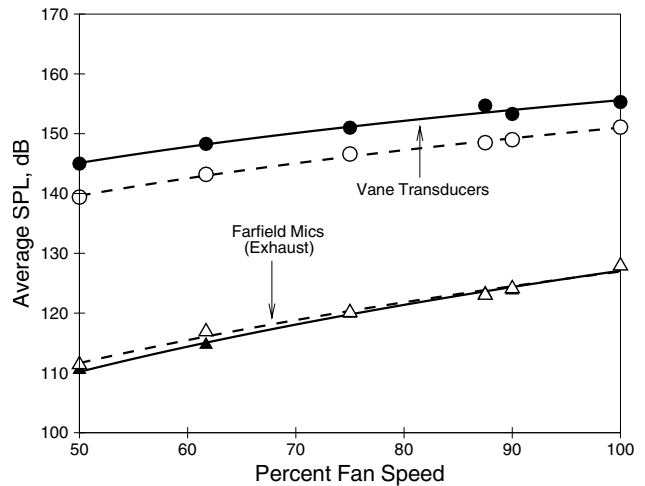


Figure B8. Same as Figure B7 but with the swept vane results shown.

References

1. Curtis, A.R.D., "Active Control of Fan Noise by Vane Actuators," NASA/CR—1999-209156, 1999.
2. Hughes, C.E., "Aerodynamic Performance of Scale-Model Turbofan Outlet Guide Vanes Designed for Low Noise," AIAA Paper 2002-0374, January 2002.
3. Hughes, C.E., Jeracki, R.J., and Miller, C.J., "Fan Noise Source Diagnostic Test—Rotor-Alone Nacelle Aerodynamic Performance Results," AIAA-Paper 2002-2426, June 2002.
4. Podboy, G.G., Krupar, M.J., Helland, S.M., and Hughes, C.E., "Steady and Unsteady Flow Field Measurements within a NASA 22 Inch Fan Model," AIAA Paper 2002-1033, January 2002.
5. Podboy, G.G. and Helland, S.M., "Fan Noise Source Diagnostic Test—Two-Point Hot-Wire Results," AIAA paper 2002-2431, June 2002.
6. Premo, J.W., "Fan Noise Source Diagnostic Test—Circumferential Mode Measurements," AIAA Paper 2002-2429, June 2002.
7. Heidelberg, L.J., "Fan Noise Source Diagnostic Test—Tone Modal Structure results," AIAA Paper 2002-2428, June 2002.
8. Woodward, R.P., Hughes, C.E., Jeracki, R.J., and Miller, C.J., "Fan Noise Source Diagnostic Test—Farfield Acoustic Results," AIAA-Paper 2002-2427, June 2002.
9. Ganz, U.W., Joppa, P.D., Patten, T.J., and Scharpf, D.F., "Boeing 18-Inch Fan Rig Broadband Noise Test," NASA/CR—1998-208704, September 1998.
10. Envia, E. and Nallasamy, M., "Design Selection and Analysis of a Swept and Leaned Stator Concept," *Journal of Sound and Vibration*, Vol. 228, No. 4, December 1999.
11. Bendat, J.S. and Piersol, A.G., *Engineering Applications of Correlation and Spectral Analysis, Second Edition* Wiley-Interscience, Inc., New York, 1993, page 45.

REPORT DOCUMENTATION PAGE			Form Approved OMB No. 0704-0188	
Public reporting burden for this collection of information is estimated to average 1 hour per response, including the time for reviewing instructions, searching existing data sources, gathering and maintaining the data needed, and completing and reviewing the collection of information. Send comments regarding this burden estimate or any other aspect of this collection of information, including suggestions for reducing this burden, to Washington Headquarters Services, Directorate for Information Operations and Reports, 1215 Jefferson Davis Highway, Suite 1204, Arlington, VA 22202-4302, and to the Office of Management and Budget, Paperwork Reduction Project (0704-0188), Washington, DC 20503.				
1. AGENCY USE ONLY (Leave blank)		2. REPORT DATE August 2002		3. REPORT TYPE AND DATES COVERED Technical Memorandum
4. TITLE AND SUBTITLE Fan Noise Source Diagnostic Test—Vane Unsteady Pressure Results			5. FUNDING NUMBERS WU-781-30-11-00	
6. AUTHOR(S) Edmane Envia				
7. PERFORMING ORGANIZATION NAME(S) AND ADDRESS(ES) National Aeronautics and Space Administration John H. Glenn Research Center at Lewis Field Cleveland, Ohio 44135-3191			8. PERFORMING ORGANIZATION REPORT NUMBER E-13503	
9. SPONSORING/MONITORING AGENCY NAME(S) AND ADDRESS(ES) National Aeronautics and Space Administration Washington, DC 20546-0001			10. SPONSORING/MONITORING AGENCY REPORT NUMBER NASA TM-2002-211808 AIAA-2002-2430	
11. SUPPLEMENTARY NOTES Prepared for the Eighth Aeroacoustics Conference cosponsored by the American Institute of Aeronautics and Astronautics and the Confederation of European Aerospace Societies, Breckenridge, Colorado, June 17-19, 2002. Responsible person, Edmane Envia, organization code 5940, 216-433-8956.				
12a. DISTRIBUTION/AVAILABILITY STATEMENT Unclassified - Unlimited Subject Category: 71 Available electronically at http://gltrs.grc.nasa.gov This publication is available from the NASA Center for AeroSpace Information, 301-621-0390.			12b. DISTRIBUTION CODE	
13. ABSTRACT (Maximum 200 words) To investigate the nature of fan outlet guide vane pressure fluctuations and their link to rotor-stator interaction noise, time histories of vane fluctuating pressures were digitally acquired as part of the Fan Noise Source Diagnostic Test. Vane unsteady pressures were measured at seven fan tip speeds for both a radial and a swept vane configuration. Using time-domain averaging and spectral analysis, the blade passing frequency (BPF) harmonic and broadband contents of the vane pressures were individually analyzed. Significant Sound Pressure Level (SPL) reductions were observed for the swept vane relative to the radial vane for the BPF harmonics of vane pressure, but vane broadband reductions due to sweep turned out to be much smaller especially on an average basis. Cross-correlation analysis was used to establish the level of spatial coherence of broadband pressures between different locations on the vane and integral length scales of pressure fluctuations were estimated from these correlations. Two main results of this work are: (1) the average broadband level on the vane (in dB) increases linearly with the fan tip speed for both the radial and swept vanes, and (2) the broadband pressure distribution on the vane is nearly homogeneous and its integral length scale is a monotonically decreasing function of fan tip speed.				
14. SUBJECT TERMS Fan noise; Outlet guide vane; Unsteady pressure			15. NUMBER OF PAGES 23	
			16. PRICE CODE	
17. SECURITY CLASSIFICATION OF REPORT Unclassified	18. SECURITY CLASSIFICATION OF THIS PAGE Unclassified	19. SECURITY CLASSIFICATION OF ABSTRACT Unclassified	20. LIMITATION OF ABSTRACT	